

1 **Krypton-81 dating of the deep Continental Intercalaire aquifer with**
2 **implications for chlorine-36 dating**

3 Takuya Matsumoto^a, Kamel Zouari^b, Rim Trabelsi^b, Darren Hillegonds^{a,c}, Wei Jiang^{d,e},
4 Zheng-Tian Lu^{d,e}, Peter Mueller^d, Jake C Zappala^d, Luis J Araguás Araguás^a, Nicolo
5 Romeo^a, Aissa Agoun^f

6

7 a) Isotope Hydrology Section, Division of Physical and Chemical Sciences, Department of
8 Nuclear Sciences and Applications, International Atomic Energy Agency, Vienna International
9 Centre, PO Box 100, 1400 Vienna, Austria.

10 b) Laboratory of Radio-Analysis and Environment, National School of Engineers, B.P 1173-
11 University of Sfax, Tunisia

12 c) Department of Earth Sciences, University of Oxford, South Parks Road, Oxford OX1 3AN UK

13 d) Physics Division, Argonne National Laboratory, Lemont, Illinois 60439, USA

14 e) Hefei National Laboratory for Physical Sciences at the Microscale, CAS Center for Excellence
15 in Quantum Information and Quantum Physics, University of Science and Technology of China,
16 Hefei, Anhui 230026, China

17 f) Direction Générale des Ressource en Eau (DGRE), Montfleury Superieur, Tunis, Tunisia

18

19 #) Corresponding Author: Isotope Hydrology Section, Division of Physical and Chemical Sciences,
20 Department of Nuclear Sciences and Applications, International Atomic Energy Agency, Vienna
21 International Centre, PO Box 100, 1400 Vienna, Austria.

22 t.matsumoto@iaea.org

23 +43 1 2600-21759 (T)

24 +43 1 2600-7 (F)

25 **Abstract**

26 Deep groundwater samples from the Continental Intercalaire (CI) aquifer in the Northern
27 Tunisian Sahara have been analyzed for noble gases ${}^3\text{He}$, ${}^4\text{He}$, Ne and ${}^{81}\text{Kr}$, and for ${}^{14}\text{C}$
28 to better constrain the groundwater residence time of this large transboundary aquifer. Its
29 significant radiogenic ${}^4\text{He}$ content and background-level ${}^{14}\text{C}$ both indicate water older
30 than a few tens of thousands of years. Distinct helium concentrations and Ne/He ratios
31 suggest different groundwater flow paths through the Tozeur and Kebili regions. ${}^{81}\text{Kr}$ is
32 applied for the first time on the CI aquifer, providing more direct evidence for the
33 presence of old groundwater with ${}^{81}\text{Kr}/\text{Kr}$ ratios at 63% – 15% of the atmospheric value,
34 corresponding to residence times of 150 – 630 ka. These newly obtained ${}^{81}\text{Kr}$ ages enable
35 a re-evaluation of the previously reported data from the Tozeur region in order to better
36 constrain the input values of ${}^{36}\text{Cl}/\text{Cl}$ and Cl. The initial ${}^{36}\text{Cl}/\text{Cl}$ ratio is found to be 4 – 6
37 times larger than previously assumed, and the initial Cl concentration 6 – 15 times
38 smaller. The results of ${}^{81}\text{Kr}$ dating and the recalibrated ${}^{36}\text{Cl}$ dating define an eastward age
39 progression across > 500 km of flow path from the Algerian to Tunisian sections. This
40 study exemplifies the utility of ${}^{81}\text{Kr}$ not only as an independent and conservative
41 chronometer, but also as a supplemental measurement to better calibrate the parameters
42 required for other age tracers, including cosmogenic ${}^{36}\text{Cl}$ and radiogenic ${}^4\text{He}$.

43 **1. Introduction**

44 The North Western Sahara Aquifer System (NWSAS), the most important and
45 intensively exploited system in northern Africa (Baba SY, 2005; Abid et al., 2009),
46 contains a set of layers with changing facies and thickness moving from the area of the
47 Chotts towards the Saharan platform (Fig.1). Numerous multidisciplinary studies
48 including chemical, isotopic and modelling techniques have been undertaken in the

49 Continental Intercalaire (CI) aquifer within NWSAS to aid groundwater resource
50 management (Edmunds et al., 2003); (Chkir and Zouari, 2007); (Abid et al., 2009);
51 (Trabelsi et al., 2009); (Abid et al., 2010); (Abid et al., 2011); (Abid et al., 2012); (Moulla
52 et al., 2012). This deep aquifer contains water older than the 30 ka limit of radiocarbon
53 dating (e.g., Edmunds et al., 2003). ^{36}Cl analysis also suggested the presence of non-
54 renewable water (Guendouz and Michelot, 2006). In this study, we applied the ^{81}Kr dating
55 method to the deeper CI aquifer in southern Tunisia. The aquifer extends from the Saharan
56 Atlas to the extreme south of the country along 700 km of eastward flow path, towards
57 the Algerian section. The ^{36}Cl groundwater ages estimated in a previous investigation
58 range from 16 ka to 1 Ma with considerable uncertainties due to complicated chloride
59 dissolution and uncertainties in the initial $^{36}\text{Cl}/\text{Cl}$ ratios (Guendouz and Michelot, 2006).

60 The noble gas radionuclide ^{81}Kr ($T_{1/2} = 229 \pm 11$ kyr) has proven to be a reliable
61 tracer for studying groundwater ages and dynamics in the age range of 40 – 1,300 ka,
62 leading to the recognition that many deep aquifers in semi-arid and arid regions are much
63 older than the ages determined earlier by radiocarbon dating ((Collon et al., 2000);
64 (Sturchio et al., 2004); (Aggarwal et al., 2014); (Gerber et al., 2017) ; (Matsumoto et al.,
65 2018); (Yokochi et al., 2019)). The ultralow isotopic abundance of ^{81}Kr ($< 10^{-12}$) in gases
66 dissolved in groundwater can be analyzed using the Atom Trap Trace Analysis (ATTA)
67 method (e.g., (Chen et al., 1999); (Jiang et al., 2012)); (Lu et al., 2014)). We applied this
68 tracer for the first time to the Tunisian part of the CI aquifer in order to better understand
69 the age structure of this important groundwater system.

70

71 **2. Field Area**

72 The CI is the largest confined aquifer of NWSAS covering an area of about one
73 million km². Numerous studies have already been carried out to infer the hydrogeology

74 of the basin ((Castany, 1982); (Mamou et al., 2006), (Edmunds et al., 1993), (Baba SY,
75 2005)). The CI aquifer is constituted by middle Jurassic to lower Cretaceous continental
76 formations described as heterogeneous sandy units with variable clay content. The
77 geological sequence of the aquifer is differentiated into several units of detrital sediments
78 separated by clay and gypsum rich strata. The aquifer units are confined by marl and clay
79 layers of the Cenomanian age, reaching, in some areas, a thickness of more than 600 m.

80 The CI aquifer covers mainly the regions of Tozeur (or Chott basin), Kebili (or
81 Nefzaoua basin) and the extreme south (Fig. 1). It is an essential natural resource for the
82 water supply of the area. The most important production takes place in the geothermal
83 regions of Kebili and Tozeur with 1,000 L/s and 600 L/s withdrawn, respectively. In the
84 Kebili region, the water bearing bed of the CI aquifer is logged in the so-called "Kebeur
85 El Haj" formations (K.H.F) composed of alternating detrital and clayey sequences
86 (Neocomian). In the south-eastern part of the Nefzaoua in Ksar Ghilane region (CIK 1),
87 the CI aquifer is logged in the Albian formations (Ab.F). The reservoir depth ranges
88 between 700 and 2,300 m with strong artesian pressure (150 – 170 m). The water
89 temperature increases from 37°C in the recharge area to above 60°C at depth. In Tozeur
90 region, the CI aquifer is principally logged in the Sidi Aich (S.A.F) sand (Lower Aptian)
91 and Boudinar (B.D.F) formations (Barremian) at depth ranging between 1,500 and 2,500
92 m. The aquifer is confined and the majority of boreholes are characterized by an artesian
93 pressure of 60 – 200 m above the ground level and with discharge temperature of about
94 70°C.

95 Groundwater flow in the CI occurs along defined flow paths, despite the presence
96 of impeding geological structures (Fig. 1). The main flow path in Kebili basin is directed
97 from the Tunisian Dahar in south-eastern Tunisia to the north-west discharge zone (Chotts
98 region). The SE-NW flow direction highlights the flow line coming from the Lower

99 Cretaceous outcrops located on the Dahar upland. The hydrogeological settings show
100 evidence of active recharge in these outcrops through water runoff, especially evident in
101 the extreme south of Tunisia where the CI well depths in Dahar area vary from 21 m to
102 120 m, indicating shallow and highly confined conditions prevailing along the flow lines
103 towards the Nefzaoua area (Dhaoui et al., 2016a). In the Djerid basin, the principal W-E
104 groundwater flow line comes from the Algerian frontier towards the discharge zone in
105 the Gulf of Gabes. Tectonic activity has played a major role in the isolation of this aquifer
106 section from the flow coming from the extreme south of the country toward Chott Djerid
107 (Kamel et al., 2005). Only the west-east flow component coming across the Algerian-
108 Tunisian border seems to ensure hydraulic continuity between the different compartments
109 of the CI aquifer in the Djerid.

110

111 **3. Method**

112 Nine groundwater samples were collected along two flow paths from the main CI
113 hydrogeological units of the survey area in February 2015 (Fig. 1). The first SE-NW flow
114 path begins in the aquifer outcrop area and ends at Chott in the confined parts of the
115 aquifer. The second W-E flow path moves from the Algerian frontier towards the
116 discharge zone in Chott region.

117 Borehole depths range from 700 to > 2000 m (Table 1). Five boreholes were
118 sampled in the Nefzaoua basin: four from the Neocomian levels (CIK 2, CIK3, CIK 4 and
119 CIK 5) and one borehole from the Albian level (CIK 1). Four boreholes were sampled
120 from the Barremian (CIT 2 and CIT 4) and the Lower Aptian (CIT1 and CIT 3) levels in
121 the Djerid basin.

122 In order to ensure that water is representative of actual aquifer conditions, all
123 samples were collected from currently exploited wells. Temperature, pH and electrical

124 conductivity (EC) were measured *in situ*. All samples were analyzed for main chemical
125 parameters using standard methods. Analyses of cations (Ca^{2+} , Mg^{2+} , Na^+ and K^+) and
126 anions (Cl^- , SO_4^{2-} , NO_3^-) were carried out in the Laboratory of Radio-Analyses and
127 Environment (LRAE), University of Sfax. The overall detection limit for ions was 0.04
128 mg/l. The total alkalinity (as HCO_3^-) was determined by titration with 0.1 M HCl solution
129 using methyl orange and bromocresol green indicators. The reliability of the chemical
130 data was assessed by checking ion balance. Calculated charge balance errors are found to
131 be less than $\pm 5\%$.

132 Water stable isotope (^{18}O , ^2H) compositions of the groundwater samples were
133 measured by laser spectrometry (LGR DLT100) at the LRAE. The isotope contents are
134 reported in the usual δ notations relative to the Vienna standard mean ocean water
135 (VSMOW) standard. Typical analytical uncertainty of the reported values is about $\pm 0.2\text{\textperthousand}$
136 for $\delta^{18}\text{O}$ and $\pm 1.5\text{\textperthousand}$ for $\delta^2\text{H}$ (one-sigma level).

137 Samples for dissolved inorganic carbon (DIC) isotope analysis were collected in
138 500 ml stainless steel bottles to avoid any contact with the atmosphere (Peterson et al.,
139 2014). The preparation prior to analysis was carried out at IDES laboratory in Orsay. The
140 ^{14}C measurements were performed at the ARTEMIS AMS facility in Saclay according to
141 published procedures (Delqué-Količ et al., 2013). The results, expressed in percent
142 modern carbon (pMC), have been corrected for the blank level of 0.2 – 0.4 pMC
143 depending on the batch. Stable DIC isotope ratios were measured at IDES laboratory in
144 Orsay (France) using Isotopic Ratio Mass Spectrometry (IRMS, typical precision of
145 0.15‰), and reported as $\delta^{13}\text{C}$ ‰ (i.e., per mile difference from Vienna PeeDee Belemnite
146 Standard [VPDB]).

147 For noble gas isotopes, groundwater samples were collected in copper tubes and
148 isolated with pinch-off metal clamps to avoid gas exchange with the atmosphere.

149 Dissolved gases were extracted and analyzed using magnetic sector (for helium) and
150 quadrupole (for neon and argon) mass spectrometers at the Isotope Hydrology Laboratory
151 of IAEA ((Matsumoto et al., 2017)).

152 For ^{81}Kr , dissolved gases (20 – 30 L STP) were extracted from groundwater in the
153 field and stored in pressurized cylinders. Gas samples were purified by cryogenic
154 distillation and gas chromatography at the Isotope Hydrology Laboratory at IAEA to
155 produce $\sim 10 \mu\text{L}$ (STP) sized, nearly pure krypton (Hillegonds; et al., 2015), for ATTA
156 work at the Trace Radioisotope Analysis Center (TRACER), Argonne National
157 Laboratory (Lu and Mueller, 2010).

158

159 **4. Results and Discussion**

160 *Chemical Composition*

161 Results for major anions, cations and *in situ* measurements are listed with borehole
162 information in Table 1. Temperature ranges from 34°C to 72°C; the lowest value was
163 measured at the CIK 1 borehole situated in the local recharge area of Daher mountains,
164 whereas higher values were measured in the boreholes in the Tozeur basin. Groundwater
165 pH values range between 6.6 and 7.6. The measured conductivity of the groundwater
166 samples range from 2.6 to 9.9 ms/cm (i.e. TDS from ca. 2106 to 8498 mg/l). The ionic
167 composition is dominated by Ca^{2+} (246–463 mg/l), Na^+ (261–2205 mg/l), Cl^- (268–4468
168 mg/l) and SO_4^{2-} (717–1410 mg/l) (Table 1). Concentrations of Mg^{2+} (43–224 mg/l) and
169 K^+ (37–150 mg/l) are relatively lower. The dominant anions are chloride and sulphide.
170 Consequently, the groundwater samples in both Kebili and Tozeur basins belong to the
171 same water type: $\text{SO}_4\text{-Cl-Ca-Na}$. This chemical pattern corresponds to water interaction
172 with the geological formations of the basin (carbonates and various evaporites) and cation
173 exchange reactions.

174

175 *Stable isotopes of water ($\delta^{18}\text{O}$, $\delta^2\text{H}$)*

176 Stable water isotope ratios range from -8.4 ‰ to -7.2‰ for $\delta^{18}\text{O}$ and from -61.5‰
177 to -50.3‰ for $\delta^2\text{H}$. The composition of water in the area closest to the outcrop (Ksar
178 Ghilane borehole in Nefzaoua basin) is slightly more enriched in the heavy isotopes than
179 deep groundwater of CI with a mean $\delta^{18}\text{O}$ value of -8‰. These results are in agreement
180 with previous studies (Abid et al., 2009) (Edmunds et al., 2003).

181 The stable isotopes in the CI waters are compared to each other and to the overlying
182 aquifers as well as to the modern rainfall (Fig. 2). The stable isotope data lie below the
183 local meteoric water line (LMWL), and are all strongly depleted in both ^{18}O and ^2H ,
184 comparing to modern Mediterranean rainfall and also to the shallowest groundwater.
185 These observations reveal a scenario of the air mass evolution different from the present
186 day case. There is also a clear difference in stable isotope compositions between CIT and
187 CIK samples (Fig. 2). The CIT samples' $\delta^{18}\text{O}$ and $\delta^2\text{H}$ cluster around -7.7 and -56 ‰,
188 whereas the CIK samples have ratios slightly more depleted in heavy, with the exception
189 of CIK1 which showed the most enriched $\delta^{18}\text{O}$ and $\delta^2\text{H}$. This is consistent with a view
190 that the CIK and CIT samples originate from separate flow paths with different recharge
191 areas.

192

193 *Radiocarbon*

194 Radiocarbon activities and $\delta^{13}\text{C}$ values of DIC are shown in Table 1 and are
195 expressed as percent of Modern Carbon (pMC) and ‰ VPDB, respectively. CI
196 groundwater shows ^{14}C activities and $\delta^{13}\text{C}$ values varying between 0.2 and 1.9 pMC, and
197 between -10.9 ‰ and -7.9 ‰ respectively. The range of $\delta^{13}\text{C}$ values is typical for
198 groundwater–rock interaction by the incongruent dissolution of carbonate (Sacks, 1996)

199 in recharging meteoric water. Longer water residence times enhance equilibration with
200 aquifer carbonate minerals resulting in lower ^{14}C activities and $\delta^{13}\text{C}$ composition closer
201 to that of host rocks (Fontes and Garnier, 1979).

202 CI groundwater residence time is calculated using various models, taking into
203 account different geochemical processes (carbonate dissolution, soil gas CO_2 dissolution,
204 CO_2 gas-aqueous exchange, calcite, bicarbonate (HCO_3^-) exchange, gypsum dissolution
205 or cation exchange, etc.). These models could be subdivided into: (i) purely chemical
206 mixing (Tamers, 1975), (ii) isotopic mixing (Ingerson and Pearson Jr., 1964) and (iii)
207 models of chemical mixing and isotopic exchange (Fontes and Garnier, 1979) (Evans et
208 al., 1979) (Mook, 1976) (Salem et al., 1980) (Eichinger, 2016). In the present case, only
209 the “Fontes and Garnier Eq.” model takes into account the two major processes occurring
210 in the CI groundwater: gypsum dissolution and Ca/Na cation exchange reactions (Abid et
211 al., 2009). The calculated ^{14}C ages according to this model (Table 1) show residence times
212 of about 30 to 50 ka. Note that the hydrological significance of these ^{14}C ages is limited
213 as these ages are clearly older than the applicable age range of the ^{14}C method (1 – 30 ka).

214

215 *Helium and Neon*

216 Groundwater residence times exceeding the ^{14}C dating limit (i.e., > 50 ka) are also
217 qualitatively supported by the ^4He concentrations in the samples. As listed in Table 2, ^4He
218 concentrations are at $10^{-6} \text{ cm}^3\text{STP/g}$, two orders of magnitude larger than that of ^4He
219 dissolved in the air-equilibrated water at recharge. Very low $^3\text{He}/^4\text{He}$ ratios of $3 \sim 8 \times 10^{-8}$
220 suggest a long residence time to allow an accumulation of radiogenic ^4He (from U and
221 Th decay) to dominate over air-derived ^4He (Fig. 3). The concentrations of U and Th in
222 the aquifer matrix have not been measured. However, if we adopt the *in situ* ^4He
223 accumulation rate of $3.3 \times 10^{-12} \text{ cm}^3\text{STP/g/yr}$ estimated by Patterson et al. (2005) for the

224 Nubian Aquifer, lithology similar to that of the CI aquifers, accumulation times required
 225 to account the measured amount of ${}^4\text{He}$ are between 500 to 3,000 kyr (Table 2). Note that
 226 these accumulation times should be regarded as the upper limits for the groundwater
 227 residence times of respective samples, as additional ${}^4\text{He}$ flux from the underlying crust
 228 would significantly increase the ${}^4\text{He}$ accumulation rates (e.g., Aggarwal et al., 2014). In
 229 addition, ${}^3\text{He}/{}^4\text{He}$ and Ne/He ratios of the samples seem to define two distinct mixing
 230 lines (Fig. 3), suggesting that there may be a small but distinct difference in ${}^3\text{He}/{}^4\text{He}$ ratios
 231 of the radiogenic components between the samples from Kebili and Tozeur regions. This
 232 difference should reflect time-integrated Li/ (U+Th) ratios of the sources of radiogenic
 233 helium, and may be regarded as supporting evidence for that the groundwater from Kebili
 234 and Tozeur regions being hydrologically separated from each other.

235

236 *Krypton-81*

237 Concentration of ${}^{81}\text{Kr}$ in groundwater samples (Table 2) is expressed in terms of
 238 the air-normalized ratio, $R_{\text{sample}}/R_{\text{air}}$, where R_{sample} and R_{air} are the ${}^{81}\text{Kr}/\text{Kr}$ ratios of the
 239 sample and of the atmosphere, respectively. $R_{\text{sample}}/R_{\text{air}}$ ratios range from 0.15 to 0.63.
 240 With the ${}^{81}\text{Kr}$ decay constant ($\lambda_{Kr} = 3.03 \times 10^{-6} \text{ yr}^{-1}$), the age (t_{Kr}) is calculated by

$$241 \quad t_{Kr} = -\frac{1}{\lambda_{Kr}} \ln\left(\frac{R_{\text{sample}}}{R_{\text{air}}}\right)$$

242 The range of ages estimated for the samples is 420 ka to 605 ka for the Touzer region.
 243 Except for a relatively younger age of 150 ka found in the sample from Ksar Ghilan
 244 (CIK1), the samples from Kebili region also defined a narrow ${}^{81}\text{Kr}$ age range, 550 to 630
 245 ka.

246 Note that these ${}^{81}\text{Kr}$ ages are clearly much older than their ${}^{14}\text{C}$ ages, confirming the
 247 above-mentioned limitation of the ${}^{14}\text{C}$ method to provide reliable age information to the

248 target aquifers. The results also reveal the presence of external ${}^4\text{He}$ flux from the
249 continental crust, as the ${}^{81}\text{Kr}$ ages are younger than the ${}^4\text{He}$ accumulation times estimated
250 without taking into account the ${}^4\text{He}$ flux.

251 The CIK1 sample with exceptionally younger ${}^{81}\text{Kr}$ age is from the borehole tapping
252 the Albian sandstones in the Dahar uplift, where recharge from a local precipitation
253 occurs. Recent isotopic investigation indicates current contribution of the Albian
254 sandstones outcrops on the Dahar in the recharge of CI aquifer by direct rainwater
255 infiltration (Dhaoui et al., 2016b). This notion is also supported by the $\delta^{18}\text{O}$ and $\delta^2\text{H}$ data
256 in which the CIK1 sample showed values intermediate between the local precipitation
257 and the rest of the CIK samples (Fig. 2).

258

259 *Chlorine-36 and Krypton-81*

260 Figure 4 compares the present ${}^{81}\text{Kr}$ ages from the Tozeur area with the previously
261 published ${}^{36}\text{Cl}$ ages from the Algerian part of the CI aquifer (Guendouz and Michelot,
262 2006). ${}^{36}\text{Cl}$ has a half-life of 301 kyr, thus it can also cover the age range older than the
263 radiocarbon limit. However, its application is generally complicated by uncertainties in
264 the initial ${}^{36}\text{Cl}/\text{Cl}$ ratio and a complex subsurface production of nucleogenic ${}^{36}\text{Cl}$ as well
265 as chloride dissolution within the aquifer (Michelot et al., 1989). As shown in Fig 4, the
266 resulting ${}^{36}\text{Cl}$ ages show significant variabilities depending on assumptions made for the
267 age calculation (Guendouz and Michelot, 2006).

268 As shown in Fig. 1, sampling points for the previous ${}^{36}\text{Cl}$ analyses (Guendouz and
269 Michelot, 2006) and those for ${}^{81}\text{Kr}$ analyses from Tozeur area are considered to be from
270 the same flow path from the recharge zone (the Saharan Atlas) to the discharge zone at
271 the Tozeur area. The ${}^{81}\text{Kr}$ data define a narrow range of ages at the discharge, but the age
272 progression from the Algerian section to the Tunisian section can only be crudely defined

273 (Fig. 4). Some ^{36}Cl ages (> 1 Ma) in the Algerian section seem overestimated, suggesting
 274 that the assumptions in the ^{36}Cl age calculation do not adequately represent the actual
 275 conditions.

276 Among the samples analyzed for ^{81}Kr , there are six wells where $^{36}\text{Cl}/\text{Cl}$ and Cl contents
 277 are also available (three sites from the Tozeur section from Petersen et al., 2014, and three
 278 sites from the Kebili section from Petersen et al., 2018). As shown in Fig. 5(a), the ^{81}Kr
 279 ages and $^{36}\text{Cl}/\text{Cl}$ ratios define a negative correlation as expected from similar decay
 280 constants of ^{81}Kr and ^{36}Cl . Age-dependent progression of Cl contents is also obvious in
 281 samples from Tozeur section, indicating an effect of chloride dissolution within aquifer
 282 (Fig. 5(b)). Chloride contents in samples from Kebili section are generally higher than
 283 those in samples from Tozeur area and showed no systematic variation. Boreholes in the
 284 Kebili section show a recent salinity increase (of 30% percent over the previous ten years)
 285 believed to be caused by intensive exploitation and consequent upward leakage from deep
 286 layers (probably the Jurassic). Thus, the Cl isotope system seems to be disturbed in the
 287 samples from Kebili section.

288 ^{36}Cl ages can be calculated by using a general equation which takes into account
 289 (1) radioactive decay of ^{36}Cl derived from the meteoric-epigene input, (2) the *in situ*
 290 production of ^{36}Cl by thermal neutron capture ($^{35}\text{Cl}(\text{n},\gamma)^{36}\text{Cl}$) within the aquifer and (3)
 291 chloride dissolution within the aquifer:

292
$$^{36}\text{R}_{\text{Meas}}[\text{Cl}]_{\text{Meas}} = ^{36}\text{R}_i[\text{Cl}]_i e^{-\lambda t} + ^{36}\text{R}_e[\text{Cl}]_i(1 - e^{-\lambda t}) + ^{36}\text{R}_e([\text{Cl}]_{\text{Meas}} - [\text{Cl}]_i)$$

 293 where λ is the decay constant of ^{36}Cl (2.303×10^{-6} yr $^{-1}$), t is the time elapsed since the
 294 recharge, $^{36}\text{R}_{\text{Meas}}$ is the measured $^{36}\text{Cl}/\text{Cl}$ ratio, $^{36}\text{R}_i$ is the initial $^{36}\text{Cl}/\text{Cl}$ ratio (= the
 295 meteoric-epigene input), $^{36}\text{R}_e$ is the $^{36}\text{Cl}/\text{Cl}$ ratio of the thermal neutron capture which is
 296 considered to be under secular equilibrium when radioactive decay of meteoric ^{36}Cl and
 297 *in situ* production of ^{36}Cl are balanced, $[\text{Cl}]_{\text{Meas}}$ is the measured Cl content, $[\text{Cl}]_i$ is the

298 initial chloride concentration. The simplest way for age calculation is to assume $[Cl]_{Meas}$
299 $= [Cl]_i$ (no chloride dissolution within the aquifer), $^{36}R_e = 5 \times 10^{-15}$ (adopted from a secular
300 equilibrium value) (Fabryka-Martin et al., 1987) (Lehmann et al., 2003), and $^{36}R_i = 116$
301 $\times 10^{-15}$ which is estimated by Guendouz and Michelot (2006) based on a theoretical value
302 of the natural ^{36}Cl fallout rate at the Saharan Atlas (Lal and Peters, 1967); (Parrat et al.,
303 1996) and the average chloride content in precipitation. These simplifications yielded ^{36}Cl
304 ages significantly older than the respective ^{81}Kr ages (Table 3), suggesting that the
305 assumptions are not applicable for these samples. Indeed, the chloride contents of the
306 Tozeur samples are in the range of *ca.* 200 to 500 mg/L and generally high compared with
307 chloride in young groundwater estimated to be about 85 mg/l in the Dahar recharge area
308 in Tunisia (Dhaoui et al., 2016). The chloride concentrations have been reported to
309 increase from the outcrops in the Atlas Mountains to the east along the transect, implying
310 the progressive dissolution of non-marine evaporates along the flow lines (Edmunds et
311 al., 2003). The calculated initial $^{36}Cl/Cl$ ratios are also based on a mean annual
312 precipitation of the recharge area, an evapotranspiration rate, and a chloride concentration
313 in precipitation for the present-day arid conditions. It is highly likely that these conditions
314 have changed with time, thus are not adaptable for age calculation (Trauth et al., 2009).

315 Instead of using those assumptions, we applied a pragmatic approach, using the ^{81}Kr
316 data for the calibration of input parameters in the ^{36}Cl age calculation by finding the initial
317 $^{36}Cl/Cl$ ratio and Cl concentration that yield a ^{36}Cl age matching the ^{81}Kr age. The balance
318 between the initial and the measured Cl is reached by contribution along the flow path
319 due to evaporite dissolution. We assume that the subsurface evaporites in question were
320 formed more than 1.5 Myr ago; ^{36}Cl initially deposited has thus decayed to a level below
321 the AMS detection limits. The results of our calculation are listed in Table 3. In order to
322 force each groundwater sample to have a residence time determined by ^{81}Kr , it appears

323 that (1) the initial $^{36}\text{Cl}/\text{Cl}$ ratio needs to be higher than the commonly assumed value by
324 a factor of 3 to 6, and (2) initial chloride contents should be much lower than those
325 observed (i.e., 50-80 mg/L in the calculation vs. 300-1200 mg/L determined
326 experimentaly). Considering the uncertainties associated with $^{36}\text{Cl}/\text{Cl}$, Cl and ^{81}Kr , these
327 samples yielded rather consistent initial $^{36}\text{Cl}/\text{Cl}$ ratios and Cl contents with averaged
328 values of $440 \pm 140 \times 10^{-15}$ and 67 ± 15 mg/L for the Tozeur section, and of $740 \pm 80 \times$
329 10^{-15} and 50 ± 26 mg/L for the Kebili section. These values are close to those found by
330 Dhaoui et al. (2016) in the recharge water in Dahar Mountains in south-eastern part of
331 Tunisia.

332 The measurement of ^{36}Cl in the meteoric proxy archives of ice cores (Baumgartner
333 et al., 1998; Wagner et al., 2001) and fossil rat urine (Plummer et al., 1997) showed that
334 the cosmogenic production rate of ^{36}Cl can vary by a factor of two. In addition, the $^{36}\text{Cl}/\text{Cl}$
335 ratio of atmospheric deposition can vary as a result of change in the stable Cl deposition
336 (Phillips, 2015), which can be produced by variation in the distance between the aquifer
337 recharge and the ocean, driven by sea-level changes. Davis et al (2003) reported that
338 meteoric $^{36}\text{Cl}/\text{Cl}$ ratios vary from 50×10^{-15} in near ocean areas to $>1000 \times 10^{-15}$ in
339 continental interior. Thus, the initial $^{36}\text{Cl}/\text{Cl}$ ratio in recharging water could differ from
340 the theoretical ratio derived from the present-day environment by more than a factor of
341 two, and the initial $^{36}\text{Cl}/\text{Cl}$ of about 400×10^{-15} is feasible.

342 Figure 4 also shows the recalculation of ^{36}Cl ages for the Algerian section of the
343 aquifer with the initial $^{36}\text{Cl}/\text{Cl}$ and Cl values calibrated for the Tozeur section with the
344 ^{81}Kr ages. Although these newly calculated ages generally agree with the previously
345 determined age ranges by Guendouz and Michelot (2006), the assumptions used here are
346 very different from the previous work. For example, the maximum ^{36}Cl ages were
347 calculated based on the assumed initial $^{36}\text{Cl}/\text{Cl}$ ratio of 133×10^{-15} and the secular

348 equilibrium $^{36}\text{Cl}/\text{Cl}$ ratio of 8×10^{-15} , presumably without taking into account the chloride
349 dissolution within the aquifer. However, we note that the chloride dissolution is a very
350 important process that needs to be assessed properly for reliable ^{36}Cl age estimation, as it
351 is obvious from Fig. 5b that this sub-surface process largely controls total Cl content. The
352 ages calculated without taking this process into account obviously overestimate the ages,
353 yielding unrealistically old groundwater ages beyond 1 Ma in areas closer to the presumed
354 recharge zone than the Tunisian section of the west to east flow line. With these ^{81}Kr -
355 calibrated ^{36}Cl ages, we narrow the possible age ranges significantly, the age progression
356 from the recharge to the east over > 500 km of transect much clearer. Accordingly, we
357 suggest that the west-to-east flow velocity is closer to 1 m/yr, much higher than the
358 previously calculated velocity of 0.5 m/yr.

359

360 **5. Conclusion and Outlook**

361 The obtained ^{81}Kr ages constitute robust and reliable data needed for the calibration
362 of numerical flow models of the CI aquifer, which in turn allow the assessment of
363 potential sustainability of this major water supply in the medium- and long-terms. CI
364 groundwater should be regarded as non-renewable, “fossil” water. The absence of any
365 current recharges presents a major issue for the effective management, sustainable
366 conservation and protection of this transboundary groundwater resource.

367 Besides these direct implications, the ^{81}Kr ages permit us to calibrate the initial
368 $^{36}\text{Cl}/\text{Cl}$ and Cl contents (thus the effect of chloride dissolution) in individual samples,
369 revealing the groundwater age structure of the CI aquifer. The procedure presented in this
370 work still ignores the possible addition of ^{36}Cl from precipitation within the last ~ 1 Ma,
371 which would result in underestimated ^{36}Cl ages. We also do not consider potential
372 subsurface production of ^{36}Cl , as identified in the Nubian aquifer (Sherif et al., 2019). In

373 addition, provided that our estimate of the initial $^{36}\text{Cl}/\text{Cl}$ is about twice as large as $^{36}\text{Cl}/\text{Cl}$
374 in the present-day soil samples from the near recharge area (Guendouz and Michelot,
375 2006), it is probable that $^{36}\text{Cl}/\text{Cl}$ ratios can vary through the entire recharge history of the
376 CI aquifer. Indeed, there are several processes that complicate the application of ^{36}Cl
377 chronometer in groundwater dating (e.g., Phillips, 2015). This study demonstrates the
378 utility of ^{81}Kr , not only to provide independent and conservative age information, but also
379 to enhance use of ^{36}Cl data. Accumulation of data on Cl isotopes and concentrations from
380 different aquifers, supported by firm chronological constraints from ^{81}Kr , should lead
381 understanding of temporal and geographical variation in $^{36}\text{Cl}/\text{Cl}$ ratios as well as
382 additional (subsurface) processes that influence the ^{36}Cl chronometer.

383

384

385 **Acknowledgements**

386 This work was carried out as a part of the IAEA's Coordinated Research Projects on Use
387 of Long-lived Radionuclides for Dating Very Old Groundwaters (IAEA CRP F33023)
388 and an associated research contract (TUN - 20813: The Use of Long-Lived Radionuclides
389 and Noble Gases for the Assessment of Groundwater Dynamics and Age of Deep Aquifer
390 Systems in Southern Tunisia). JCZ, WJ, ZTL and PM acknowledge that this material is
391 based upon work supported by Laboratory Directed Research and Development (LDRD)
392 funding from Argonne National Laboratory, provided by the Director, Office of Science,
393 of the U.S. Department of Energy under Contract No. DE-AC02-06CH11357. The
394 authors wish to thank the staff members of Water Resources Divisions in Tozeur and
395 Kebili for their help during fieldwork. They are grateful to LRAE laboratory for support
396 provided for the chemical and isotope analysis. Melissa Denecke is also thanked for
397 comments and suggestions on the manuscript.

398

399 **References**

400 Abid, K., Ammar, F.H., Chkir, N. and Zouari, K. (2012) Relationship between Senonian
401 and deep aquifers in Southern Tunisia. *Quaternary International* 257, 13-26.

402 Abid, K., Trabelsi, R.I.M., Zouari, K. and Abidi, B. (2009) Caractérisation
403 hydrogéochimique de la nappe du Continental Intercalaire (sud tunisien) /
404 Hydrogeochemical characterization of the Continental Intercalaire aquifer
405 (southern Tunisia). *Hydrological Sciences Journal* 54, 526-537.

406 Abid, K., Zouari, K. and Abidi, B. (2010) Identification and characterisation of
407 hydrogeological relays of continental intercalaire aquifer of southern
408 Tunisia. *Carbonates and Evaporites* 25, 65-75.

409 Abid, K., Zouari, K., Dulinski, M., Chkir, N. and Abidi, B. (2011) Hydrologic and
410 geologic factors controlling groundwater geochemistry in the Turonian
411 aquifer (southern Tunisia). *Hydrogeology Journal* 19, 415-427.

412 Abid, K., Ammar, F.H., Chkir, N. and Zouari, K. (2012) Relationship between Senonian
413 and deep aquifers in Southern Tunisia. *Quaternary International* 257, 13-26.

414 Aggarwal, P.K., Matsumoto, T., Sturchio, N.C., Chang, H.K., Gastmans, D., Araguas-
415 Araguas, L.J., Jiang, W., Lu, Z.-T., Mueller, P., Yokochi, R., Purtschert, R.
416 and Torgersen, T. (2014) Continental degassing of ${}^4\text{He}$ by surficial
417 discharge of deep groundwater. *Nature Geoscience* 8, 35.

418 Baba SY, M.O. (2005) Recharge et paleorecharge du systeme aquifere du sahara
419 septentrional Faculte des Sciences de Tunis Universite de Tunis el Manar
420 Tunis, p. 261.

421 Castany, G. (1982) Bassin sédimentaire du Sahara septentrional (Algérie Tunisie).
422 Aquifères du Continental Intercalaire et du Complexe Terminal.
423 Bull. BRGM 2, 127-147.

424 Chen, C.Y. Y.M. Li, K. Bailey, T.P. O'Connor, L. Young, Z.-T. Lu (1999) Ultrasensitive
425 isotope trace analyses with a magneto-optical trap, *Science* **286**, 1139.

426 Chkir, N. and Zouari, K. (2007) Uranium isotopic disequilibrium for groundwater
427 classification: first results on complexe terminal and continental intercalaire
428 aquifers in Southern Tunisia. *Environmental Geology* **53**, 677-685.

429 Collon, P., Kutschera, W., Loosli, H.H., Lehmann, B.E., Purtschert, R., Love, A.,
430 Sampson, L., Anthony, D., Cole, D., Davids, B., Morrissey, D.J., Sherrill,
431 B.M., Steiner, M., Pardo, R.C. and Paul, M. (2000) Kr-81 in the Great
432 Artesian Basin, Australia: a new method for dating very old groundwater.
433 *Earth and Planetary Science Letters* **182**, 103-113.

434 Delqué-Količ, E., Comby-Zerbino, C., Ferkane, S., Moreau, C., Dumoulin, J.P., Caffy,
435 I., Souprayen, C., Quilès, A., Bavay, D., Hain, S. and Setti, V. (2013)
436 Preparing and measuring ultra-small radiocarbon samples with the
437 ARTEMIS AMS facility in Saclay, France. *Nuclear Instruments and*
438 *Methods in Physics Research Section B: Beam Interactions with Materials*
439 and Atoms

440 294, 189-193.

441 Dhaoui, Z., Zouari, K., Taupin, J.-D. and Farouni, R. (2016a) Hydrochemical and isotopic
442 investigations as indicators of recharge processes of the Continental
443 Intercalaire aquifer (eastern piedmont of Dahar, southern Tunisia).
444 *Environmental Earth Sciences* **75**, 1-14.

445 Dhaoui, Z., Zouari, K., Taupin, j.d. and Farouni, R. (2016b) Hydrochemical and isotopic
446 investigations as indicators of recharge processes of the Continental
447 Intercalaire aquifer (eastern piedmont of Dahar, southern Tunisia).

448 Edmunds, W.M., Guendouz, A.H., Mamou, A., Moulla, A., Shand, P. and Zouari, K.
449 (2003) Groundwater evolution in the Continental Intercalaire aquifer of

449 southern Algeria and Tunisia: trace element and isotopic indicators. Applied
450 Geochemistry 18, 805-822.

451 Edmunds, W.M., Shand, P., Guendouz, A.H., Moulla, A.S., Mamou, A. and Zouari, K.
452 (1993) Recharge Characteristics and Groundwater Quality of the Grand Erg
453 Oriental Basin.

454 Eichinger, L. (2016) A Contribution to the Interpretation of ^{14}C Groundwater Ages
455 Considering the Example of a Partially Confined Sandstone Aquifer.
456 Radiocarbon 25, 347-356.

457 Evans, G.V., Otlet, R.L., Downing, R.A., Monkhouse, R.A. and Rae, G. (1979) Some
458 problems in the interpretation of isotope measurements in United Kingdom
459 aquifers. IAEA, International Atomic Energy Agency (IAEA).

460 Fabryka-Martin, J., Davis, S.N. and Elmore, D. (1987) Applications of ^{129}I and ^{36}Cl in
461 hydrology. Nuclear Instruments and Methods in Physics Research Section
462 B: Beam Interactions with Materials and Atoms 29, 361-371.

463 Fontes, J.-C. and Garnier, J.-M. (1979) Determination of the initial ^{14}C activity of the
464 total dissolved carbon: A review of the existing models and a new approach.
465 Water Resources Research 15, 399-413.

466 Gerber, C., Vaikmae, R., Aeschbach, W., Babre, A., Jiang, W., Leuenberger, M., Lu, Z.-T.,
467 Mokrik, R., Mueller, P., Raidla, V., Saks, T., Niklaus Waber, H., Weissbach, T.,
468 Zappala, J., Purtschert, R. (2017) Using ^{81}Kr and noble gases to characterize and
469 date groundwater and brines in the Baltic Artesian Basin on the one-million-year
470 timescale, Geochimica et Cosmochimica Acta 205, 187-210

471

472 Guendouz, A. and Michelot, J.L. (2006) Chlorine-36 dating of deep groundwater from
473 northern Sahara. Journal of Hydrology 328, 572-580.

474 Hillebrands;, D., Matsumoto;, T. and Romeo;, N. (2015) Krypton isolation and
475 purification from groundwater for 81Kr age dating, International
476 Symposium on Isotope Hydrology: Revisiting Foundations and Exploring
477 Frontiers, International Atomic Energy Agency, Vienna, Austria, p. pp.49.

478 Ingerson, E. and Pearson Jr., F.J. (1964) Estimation of age and rate of motion of ground
479 water by the 14C method. Recent Researches in the fields of Hydrosphere.
480 Atmosphere and Nuclear Chemistry, 263–283.

481 Jiang, W., K. Bailey, Z.-T. Lu*, P. Mueller, T.P. O'Connor, C.-F. Cheng, S.-M. Hu, R.
482 Purtschert, N.C. Sturchio, Y.R. Sun, W. D. Williams, and G.-M. Yang
483 (2012) An atom counter for measuring ^{81}Kr and ^{85}Kr in environmental
484 samples, *Geochimica et Cosmochimica Acta* **91**, 1-6

485 Kamel, S., Dassi, L., Zouari, K. and Abidi, B. (2005) Geochemical and isotopic
486 investigation of the aquifer system in the Djerid-Nefzaoua basin, southern
487 Tunisia. *Environmental Geology* **49**, 159-170.

488 Lal, D. and Peters, B. (1967) Cosmic Ray Produced Radioactivity on the Earth, in: Sitte,
489 K. (Ed.), *Kosmische Strahlung II / Cosmic Rays II*. Springer Berlin
490 Heidelberg, Berlin, Heidelberg, pp. 551-612.

491 Lehmann, B.E., Love, A., Purtschert, R., Collon, P., Loosli, H.H., Kutschera, W.,
492 Beyerle, U., Aeschbach-Hertig, W., Kipfer, R., Frape, S.K., Herczeg, A.,
493 Moran, J., Tolstikhin, I.N. and Gröning, M. (2003) A comparison of
494 groundwater dating with 81Kr , 36Cl and 4He in four wells of the Great
495 Artesian Basin, Australia. *Earth and Planetary Science Letters* **211**, 237-
496 250._

497 Lu, Z.-T., P. Schlosser, W.M. Smethie Jr., N.C. Sturchio, T.P. Fischer, B.M. Kennedy,
498 R. Purtschert, J.P. Severinghaus, D.K. Solomon, T. Tanhua, R. Yokochi

499 (2014), Tracer Applications of Noble Gas Radionuclides in the
500 Geosciences, *Earth-Science Reviews* **138**, 196-214.

501 Mamou, A., Besbes, M., Abdous, B., Latrech, D.J. and Fezzani, C. (2006) North-Western
502 Sahara Aquifer System (NWSAS), in: Foster, S., Loucks, D.P. (Eds.), Non-
503 renewable Groundwater Resources: A guidebook on socially sustainable
504 management for water-policy makers. United Nations Educational,
505 Scientific and Cultural Organization, Paris, pp. 68-74.

506 Matsumoto, T., Chen, Z., Wei, W., Yang, G.-M., Hu, S.-M. and Zhang, X. (2018)
507 Application of combined ^{81}Kr and ^4He chronometers to the dating of old
508 groundwater in a tectonically active region of the North China Plain. *Earth*
509 and *Planetary Science Letters* **493**, 208-217.

510 Matsumoto, T., Silomon, K.D., Araguás-Araguás, L. and Aggarwal, P. (2017) The
511 IAEA's Coordinated Research Project on ``Estimation of Groundwater
512 Recharge and Discharge by Using the Tritium, Helium-3 Dating
513 Technique": In Lieu of a Preface. *Geochemical Journal* **51**, 385-390.

514 Michelot, J., Fontes, J., Soreau, S., Lehmann, B., Loosli, H., Balderer, W., Elmore, D.,
515 Kubik, P., Wolfli, W., Beer, J. and Synal, A. (1989) Chlorine-36 in deep
516 groundwaters and host-rocks of northern Switzerland; sources, evolution
517 and hydrological implications. *Water-Rock Interaction*, 483-486.

518 Mook, W.G. (1976) The dissolution-exchange model for dating groundwater with ^{14}C .
519 IAEA, International Atomic Energy Agency (IAEA).

520 Moulla, A.S., Guendouz, A., Cherchali, M.E.H., Chaid, Z. and Ouarezki, S. (2012)
521 Updated geochemical and isotopic data from the Continental Intercalaire
522 aquifer in the Great Occidental Erg sub-basin (south-western Algeria).
523 *Quaternary International* **257**, 64-73.

524 Parrat, Y., Hajdas, W., Baltensperger, U., Synal, H.A., Kubik, P.W., Suter, M. and
525 Gäggeler, H.W. (1996) Cross section measurements of proton induced reactions
526 using a gas target. Nuclear Instruments and Methods in Physics Research Section
527 B: Beam Interactions with Materials and Atoms 113, 470-473.

528 Petersen, J.O., Deschamps, P., Gonçalvès, J., Hamelin, B., Michelot, J.L., Guendouz, A.
529 and Zouari, K. (2014) Quantifying paleorecharge in the Continental Intercalaire
530 (CI) aquifer by a Monte-Carlo inversion approach of $^{36}\text{Cl}/\text{Cl}$ data. Applied
531 Geochemistry 50, 209-221.

532 Petersen, J.O., Deschamps, P., Hamelin, B., Fourré, E., Gonçalvès, J., Zouari, K.,
533 Guendouz, A., Michelot, J.-L., Massault, M., Dapoigny, A., Team, A -
534 (2018) Groundwater flowpaths and residence times inferred by ^{14}C , ^{36}Cl
535 and ^{4}He isotopes in the Continental Intercalaire aquifer (North-Western
536 Africa), Journal of Hydrology 560,11-23.

537 Plummer, M.A., Phillips, F.M., Fabryka-Martin, J., Turin, H.J., Wigand, P.E. and
538 Sharma, P. (1997) Chlorine-36 in Fossil Rat Urine: An Archive of
539 Cosmogenic Nuclide Deposition During the Past 40,000 Years. Science
540 277, 538.

541 Sacks, L.A. (1996) Geochemical and isotopic composition of groundwater with emphasis
542 on sources of sulfate in the Upper Floridan Aquifer in Parts of Marion,
543 Sumter and Citrus Counties, Florida. US Geological Survey, water-
544 resources investigations report, 95-4251.

545 Salem, O., Visser, J.H., Dray, M. and Gonfiantini, R. (1980) Groundwater flow patterns
546 in the western Libyan Arab Jamahiriya evaluated from isotopic data. IAEA,
547 International Atomic Energy Agency (IAEA).

548 Sturchio, N.C., Du, X., Purtschert, R., Lehmann, B.E., Sultan, M., Patterson, L.J., Lu,
549 Z.T., Muller, P., Bigler, T., Bailey, K., O'Connor, T.P., Young, L., Lorenzo,
550 R., Becker, R., El Alfay, Z., El Kalioubi, B., Dawood, Y. and Abdallah,
551 A.M.A. (2004) One million year old groundwater in the Sahara revealed by
552 krypton-81 and chlorine-36. *Geophysical Research Letters* 31.

553 Tamers, M.A. (1975) Validity of radiocarbon dates on ground water. *Geophysical*
554 *Surveys* 2, 217-239.

555 Trabelsi, R., Kacem, A., Zouari, K. and Rozanski, K. (2009) Quantifying regional
556 groundwater flow between Continental Intercalaire and Djeffara aquifers in
557 southern Tunisia using isotope methods. *Environmental Geology* 58, 171-
558 183.

559 Trauth, M.H., Larrasoña, J.C. and Mudelsee, M. (2009) Trends, rhythms and events in
560 Plio-Pleistocene African climate. *Quaternary Science Reviews* 28, 399-411.

561 Yokochi, R., R. Ram, J. C. Zappala, W. Jiang, E. Adar*, R. Bernier, A. Burg, U. Dayan,
562 Z.-T. Lu*, P. Mueller, R. Purtschert, Y. Yechieli (2019). "Radiokrypton
563 unveils dual moisture sources of a deep desert aquifer." *Proceedings of the*
564 *National Academy of Sciences* **116**(33): 16222-16227.

565

566

567

568

569

570

Table 1. List of groundwater samples collected for the present study with chemical and isotope analyses results

Sample ID	Site	Aquifer Formation	Formation	Altitude (m)	Depth (m)	CE (ms/cm)	T (°C)	pH	$\delta^{18}\text{O}$ ‰	$\delta^2\text{H}$ ‰	HCO_3^-	$\text{Cl}^{(\#)}$	NO_3^-	SO_4^{2-}	Na^+	K^+	Ca^{2+}	Mg^{2+}	TDS (mg/l)	$\delta^{13}\text{C}$ ‰ (\$)	^{14}C (pmc)	^{14}C age (kyr)
<i>CIT Tozeur (CIT) Region</i>																						
CIT1	Nefta	Sidi Aich Sand	Lower Aptian	100	2160	2.8	73	7.0	-7.8	-55.2	146	296	1	1062	271	82	340	48	2212	-10.1	0.23	39
CIT2	Jhim	Boudinar Sand	Barremian	21	2507	3.0	70	7.1	-7.7	-56.8	134	530	4	1049	348	56	363	52	2536	-9.18	1.9	27
CIT3	Tozeur	Sidi Aich Sand	Lower Aptian	87	1997	3.0	65	7.4	-7.6	-56.1	134	536	10	1172	322	84	366	43	2485	-9.05	1.5	30
CIT4	Tazrarit	Boudinar Sand	Barremian	33	2186	4.8	68	6.7	-7.5	-54.1	183	414	31	1077	784	87	423	57	4042	-7.9	0.35	39
<i>CI Kébili (CIK) Region</i>																						
CIK1	Ksar Ghilane	Albian Sand/sandstone	Albian	211	667	4.18	34	7.1	-7.2	-50.3	201	1037	0	1410	740	53	443	224	4306	-10.9	0.3	45
CIK2	Douz	Kbeur El Haj Sand/Sandstone	Neocomian	70	1994	9.88	44	6.7	-8.4	-61.2	146	1188	39	876	2205	150	463	150	8498	-10.8	0.17	48
CIK3	Kébili	Kbeur El Haj Sand/Sandstone	Neocomian	58	2556	2.66	65	6.6	-8.4	-61.1	134	542	0	717	371	37	246	62	2182	-10.7	0.25	45
CIK4	Limagues	Kbeur El Haj Sand/Sandstone	Neocomian	81	1752	2.8	69	7.6	-8.3	-61.5	140	606	3	773	342	40	276	65	2245	-8	0.73	39
CIK5	Souk Lahad	Kbeur El Haj Sand/ Sandstone	Neocomian	40	2200	3.4	67	7.1	-8.3	-61	134	586	21	683	306	40	268	68	2106	-10.84	0.33	43

(#) Chloride data shown as *Italic* are adopted from Peterson et al. (2014 and 2018).

(\$) Carbon isotope data shown as *Italic* are from Petersen et al. (2018), Abid et al., (2009 and 2012).

Table 2. Results of noble gas isotope analysis.

Sample		Mass Spectrometer			ATTA	
ID	Site	He ($\times 10^{-6}$ cm 3 STP/g)	$^3\text{He}/^4\text{He}$ ($\times 10^{-8}$)	Ne ($\times 10^{-7}$ cm 3 STP/g)	$^{81}\text{Kr}/\text{Kr}$ ($R_{\text{sample}}/R_{\text{air}}$) (#)	^{81}Kr Age ($\times 10^5$ yr)
CIT1	Nefta	2.64 \pm 0.04	3.72 \pm 0.05	2.61 \pm 0.03	0.28 \pm 0.02	4.20 \pm 0.31
CIT2	Jhim	1.93 \pm 0.05	5.10 \pm 0.10	2.60 \pm 0.06	0.20 \pm 0.01	5.31 \pm 0.3
CIT3	Tozeur	3.71 \pm 0.10	4.18 \pm 0.22	3.78 \pm 0.08	0.16 \pm 0.01	6.05 \pm 0.35
CIT4	Tazrarit	4.97 \pm 0.13	3.03 \pm 0.07	2.56 \pm 0.06	0.23 \pm 0.02	4.85 \pm 0.36
CIK1	Ksar Ghilan	2.19 \pm 0.06	5.63 \pm 0.09	2.55 \pm 0.06	0.63 \pm 0.02	1.52 \pm 0.13
CIK2	Douz	9.29 \pm 0.24	3.69 \pm 0.11	4.32 \pm 0.09	0.15 \pm 0.01	6.26 \pm 0.36
CIK3	Kébili	2.01 \pm 0.05	6.43 \pm 0.15	2.56 \pm 0.06	0.17 \pm 0.01	5.85 \pm 0.33
CIK4	Limagues	1.60 \pm 0.03	7.03 \pm 0.11	2.51 \pm 0.02	0.19 \pm 0.01	5.48 \pm 0.31
CIK5	Souk Lahad	2.01 \pm 0.03	7.79 \pm 0.10	4.01 \pm 0.04	0.17 \pm 0.02	5.84 \pm 0.47

Table 3. Re-evaluation of ^{36}Cl ages with ^{81}Kr ages.

Sample ID	Site	Measured Values(\$)		^{36}Cl Age (ka) [#]	^{81}Kr Age (ka)	Calibrated Parameters by ^{81}Kr ages		
		Cl (mg/L)	$^{36}\text{Cl}/\text{Cl}$			Initial $^{36}\text{Cl}/\text{Cl}$	Initial Cl	^{36}Cl Age (ka)
CIT1	Nefta	296	2.54E-14	725	420 \pm 31	3.4E-13	50	420
CIT3	Tozeur	536	1.48E-14	1043	605 \pm 35	3.4E-13	90	605
CIT4	Tazrarit	414	3.38E-14	575	485 \pm 36	6E-13	70	485
CIK1	Ksar Ghilan	1037	4.03E-14	498	152 \pm 13	7.40E-13	80	152
CIK2	Douz	1188	5.40E-15	2450	626 \pm 36	6.60E-13	40	626
CIK3	Kébili	542	1.20E-14	1200	585 \pm 33	8.20E-13	30	585

\$) Cl isotope data are adopted from Guendouz and Michelot (2006) and Petersen et al. (2014; 2018)

#) Ages calculated with a generic initial $^{36}\text{Cl}/\text{Cl}$ and no chloride dissolution

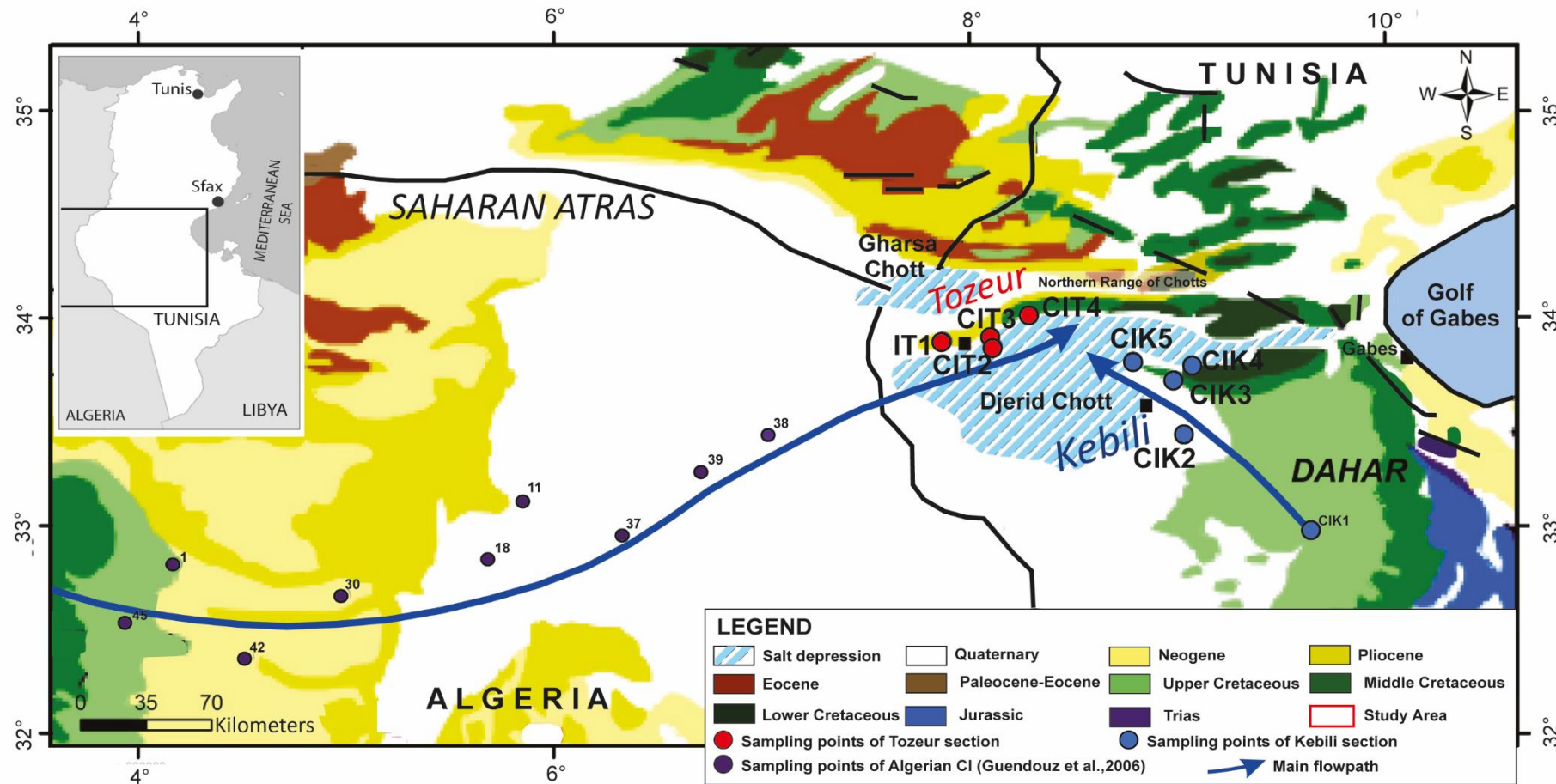


Fig.1. Geological map of the sampling points in the CI aquifer (Tozeur and Kebili sections in Tunisia). Sampling points for the previous ^{36}Cl analysis (Guendouz and Michelot, 2006) are also shown on the Algerian side of the CI aquifer.

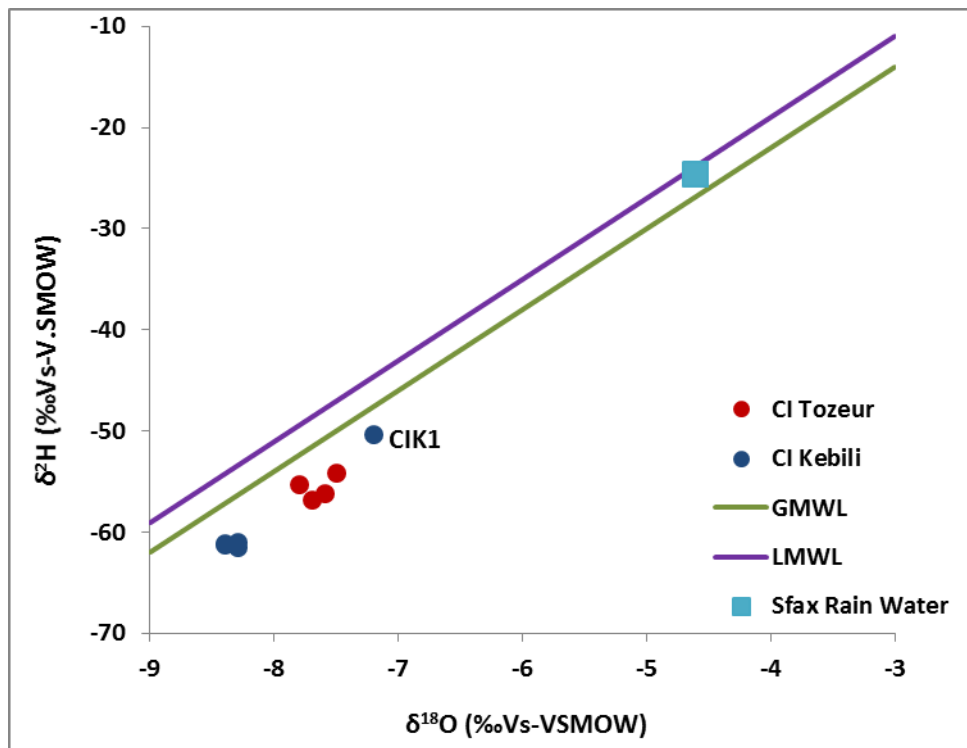


Fig. 2. $\delta^{18}\text{O}$ and $\delta^2\text{H}$ of CI groundwater in Kebili and Tozeur regions. GMWL: Global Meteoric Water Line; LMWL: Local Meteoric Water Line.

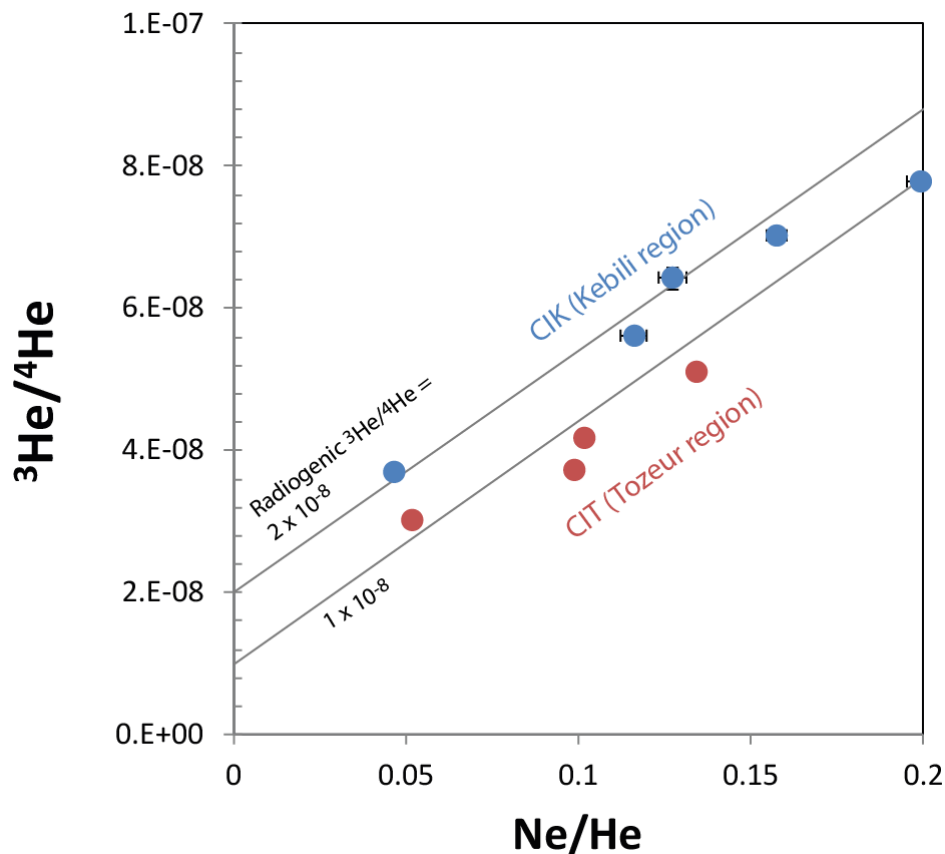


Fig. 3. Ne/He and $^{3}\text{He}/^{4}\text{He}$ ratios of the groundwater from CI aquifer in Tozeur and Kebili regions. Solid lines represent binary mixing lines between an atmospheric component and a crustal radiogenic component whose $^{3}\text{He}/^{4}\text{He}$ ratio is 1×10^{-8} or 2×10^{-8} .

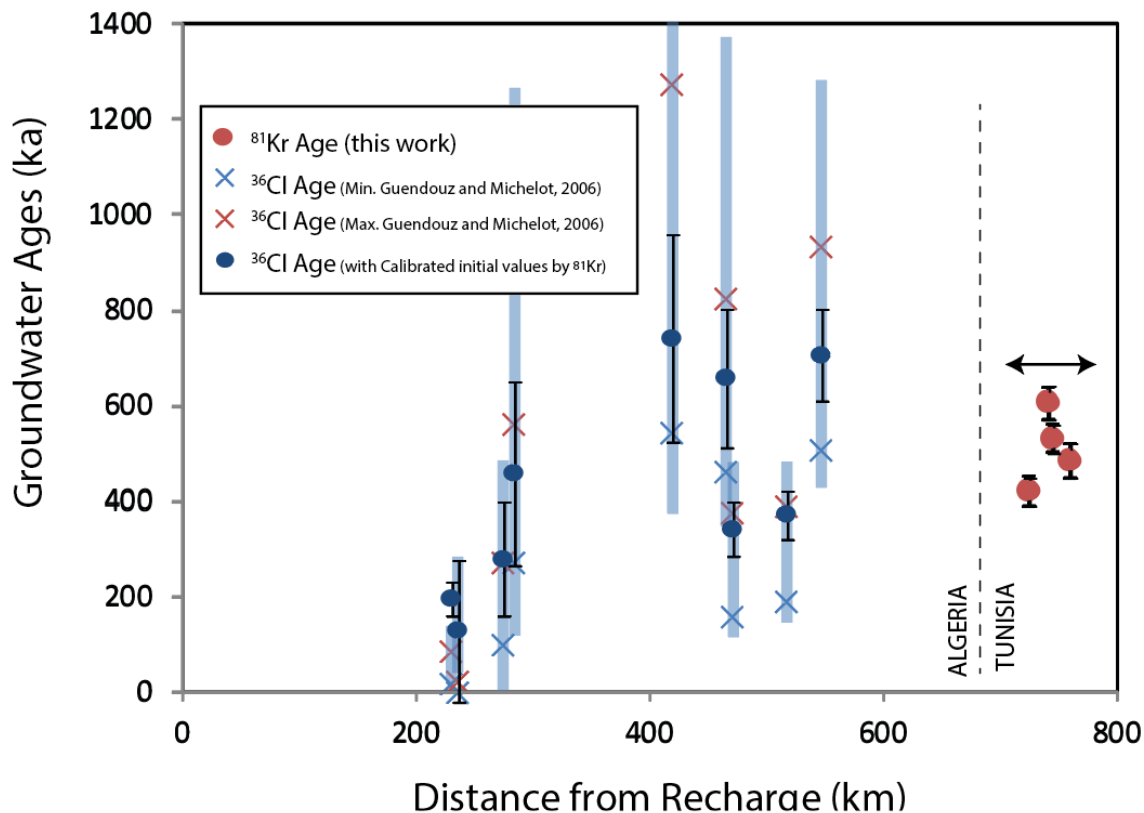


Fig. 4. ^{81}Kr ages (this study) and ^{36}Cl ages (Guendouz and Michelot, 2006; and this work) plotted against the distances from recharge. The minimum ^{36}Cl ages by Guendouz and Michelot (2006) were calculated by using $^{36}R_i = 116 \times 10^{-15}$ and $^{36}Re = 0$, and their maximum ages were obtained with $^{36}R_i = 133 \times 10^{-15}$ and $^{36}Re = 8 \times 10^{-15}$. The blue bands are to show the range that covered by the maximum and minimum ^{36}Cl ages of Guendouz and Michelot (2006) with quoted uncertainties. The ^{36}Cl ages re-evaluated based on the initial $^{36}\text{Cl}/\text{Cl}$ and Cl values calibrated with the ^{81}Kr ages are shown with blue dots (see text).

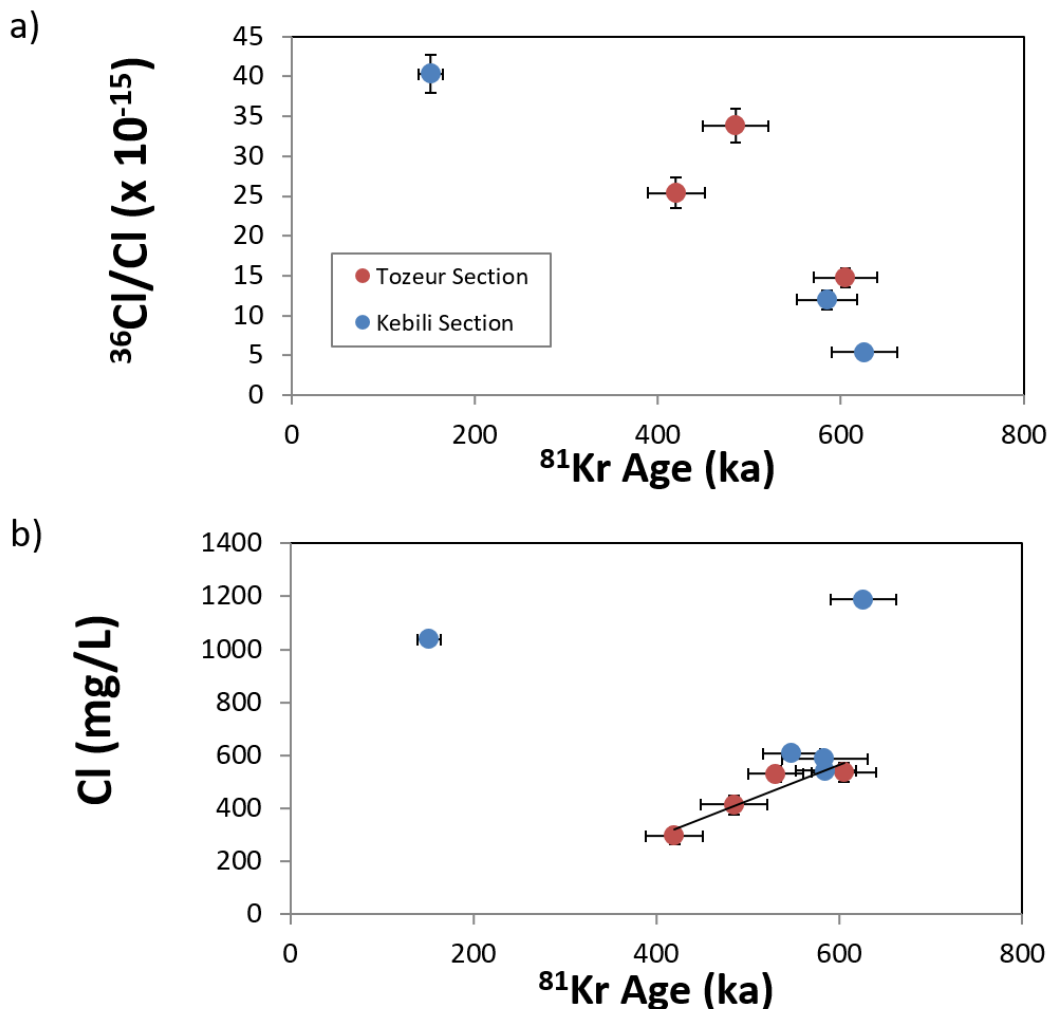


Figure 5 $^{36}\text{Cl}/\text{Cl}$ ratios and Cl contents versus ^{81}Kr ages.